

A Comprehensive View of Circumstellar Disks in Chamaeleon I: Infrared Excess, Accretion Signatures and Binarity

Ivana Damjanov¹, Ray Jayawardhana¹, Alexander Scholz²,
Mirza Ahmic¹, Duy C. Nguyen¹, Alexis Brandeker³, Marten H. van Kerkwijk¹

ABSTRACT

We present a comprehensive study of disks around 81 young low-mass stars and brown dwarfs in the nearby ~ 2 Myr-old Chamaeleon I star-forming region. We use mid-infrared photometry from the *Spitzer Space Telescope*, supplemented by findings from ground-based high-resolution optical spectroscopy and adaptive optics imaging. We derive disk fractions of $52\% \pm 6\%$ and $58_{-7}^{+6}\%$ based on $8\ \mu\text{m}$ and $24\ \mu\text{m}$ colour excesses, respectively, consistent with those reported for other clusters of similar age. Within the uncertainties, the disk frequency in our sample of K3–M8 objects in Cha I does not depend on stellar mass. Diskless and disk-bearing objects have similar spatial distributions. There are no obvious transition disks in our sample, implying a rapid timescale for the inner disk clearing process; however, we find two objects with weak excess at $3\text{--}8\ \mu\text{m}$ and substantial excess at $24\ \mu\text{m}$, which may indicate grain growth and dust settling in the inner disk. For a sub-sample of 35 objects with high-resolution spectra, we investigate the connection between accretion signatures and dusty disks: in the vast majority of cases (29/35) the two are well correlated, suggesting that, on average, the timescale for gas dissipation is similar to that for clearing the inner dust disk. The exceptions are six objects for which dust disks appear to persist even though accretion has ceased or dropped below measurable levels. Adaptive

¹Department of Astronomy and Astrophysics, University of Toronto, 50 St. George Street, Toronto, ON M5S 3H4, Canada; damjanov@astro.utoronto.ca.

²School of Physics & Astronomy, University of St. Andrews, North Haugh, St. Andrews, Fife KY16 9SS United Kingdom.

³Stockholm Observatory, AlbaNova University Center, Stockholms Center for Physics, Astronomy and Biotechnology, Roslagstullsbacken 21, SE-106 91 Stockholm, Sweden.

optics images of 65 of our targets reveal that 17 have companions at (projected) separations of 10–80 AU. Of the five $\lesssim 20$ AU binaries, four lack infrared excess, possibly indicating that a close companion leads to faster disk dispersal. The closest binary with excess is separated by ~ 20 AU, which sets an upper limit of ~ 8 AU for the outer disk radius. The overall disk frequency among stars with companions ($35^{+15}_{-13}\%$) is lower than (but still statistically consistent with) the value for the total sample.

Subject headings: Accretion, Accretion Disks – Circumstellar Matter – Planetary Systems – Stars: Low Mass, Brown Dwarfs – Binaries: General

1. Introduction

Circumstellar disks are a natural outcome of star formation and the potential birth sites of planets. Thus studies of disk evolution can provide useful constraints on both pre-main-sequence stellar evolution and planet formation timescales. Dusty disks may be identified most easily by their infrared emission. Observations in the mid-infrared are much more sensitive to disks than those in the near-infrared, since the stellar photospheric flux declines rapidly at longer wavelengths while the disk emission rises. The *Spitzer Space Telescope*, with its Infrared Array Camera (IRAC) and Multiband Imaging Photometer (MIPS) operating in the 3.6–160 μm range, has greatly improved our ability to identify and study disks surrounding young stars (e.g., Hartmann et al. 2005; Sicilia-Aguilar et al. 2006; Lada et al. 2006). Processes of grain growth and dust settling to the midplane, along with the possible formation of planetesimals, are thought to occur in the inner disks. The consequent reduction of small dust grain abundance results in weak or absent near-infrared emission but the mid- to far-infrared disk emission remains strong, leading to the characteristic signature of “transition disks” (D’Alessio et al. 2005; Calvet et al. 2005; Muzerolle et al. 2006). The spectral energy distribution (SED) in 4–25 μm wavelength range is thus ideal for probing dust in the inner disk.

Since gas constitutes most ($\sim 99\%$) of the disk mass and is essential for building giant planets, it is important to know whether gas and dust disperse on similar timescales. While it is difficult to detect the bulk of the disk gas directly, its presence can be inferred from signatures of accretion from the inner disk edge onto the central star. The most prominent signature of infalling gas is a broad, asymmetric and strong $\text{H}\alpha$ emission line (Mohanty et al. 2005; Muzerolle et al. 2005; Jayawardhana et al. 2006). A comparison between accretion signatures and infrared emission can reveal whether the timescales for dust and gas dissipation are similar. Another important question related to planet formation is whether the presence

of a binary companion has a considerable effect on disk evolution (Bouwman et al. 2006, and references therein).

Here we present a comprehensive study of disks surrounding 81 stars and brown dwarfs in the nearby (160 pc; Whittet et al. 1997), young (~ 2 Myr; Luhman 2004, and references therein) Chamaeleon I cloud (abbreviated Cha I in the following), using *Spitzer* IRAC 4–8 μm and MIPS 24 μm data. We study the overall disk frequency as well as its possible dependence on stellar spectral type, and look for transition disk candidates. For 35 of the targets, for which high-resolution optical spectra are available (Nguyen et al., in prep.; Mohanty et al. 2005; Muzerolle et al. 2005), we investigate the connection between infrared excess and accretion signatures. For 65 objects –the largest such sample to date– the availability of adaptive optics images (Ahmic et al., in prep.) allows us to explore how multiplicity affects disk dissipation.

2. Spitzer Data and Photometry

We used publicly available images of the Cha I star-forming region from the IRAC and MIPS instruments aboard the *Spitzer Space Telescope* (GTO programs # 6 and 37, PI: G. Fazio). The IRAC images of the southern and northern cloud cores in Cha I at 3.6, 4.5, 5.8 and 8.0 μm were obtained in June and July 2004 (AOR keys 3960320 and 3651328). The plate scale and the spatial resolution of IRAC are $1''.2$ and $\sim 2''$, respectively (Fazio et al. 2004). For these programs, the *Spitzer* Science Center (SSC) pipeline (ver S14.0.0) provides two shallow (exp. time 20.8 s) maps for all of the four IRAC channels, each performed twice with an offset of a few arcseconds. These dual maps for the southern cloud have centers at $\alpha \approx 11^{\text{h}}07^{\text{m}}$, $\delta \approx -77^{\text{h}}34^{\text{m}}$ (J2000) for 3.6 and 5.8 μm and at $\alpha \approx 11^{\text{h}}07^{\text{m}}$, $\delta \approx -77^{\text{h}}28^{\text{m}}$ (J2000) for 4.5 and 8.0 μm . The northern cloud core maps have centers at $\alpha \approx 11^{\text{h}}09^{\text{m}}$, $\delta \approx -76^{\text{h}}36^{\text{m}}$ (J2000) for 3.6 and 5.8 μm and at $\alpha \approx 11^{\text{h}}10^{\text{m}}$, $\delta \approx -76^{\text{h}}30^{\text{m}}$ (J2000) for 4.5 and 8.0 μm . The dimensions of the maps are $33' \times 29'$. In each of the four bands, BCD images for each of the shallow maps were taken through the post-BCD pipeline at the SSC, where the pointing refinement and mosaicing with standard MOPEX tool were performed. We used these archived final post-BCD shallow mosaics for IRAC photometric measurements in our analysis.

The observations of the northern and southern Cha I cloud cores using MIPS were taken in April 2004 and February 2005 (AOR keys 3661312 and 3962112). The relevant MIPS imaging band for the purpose of this analysis is the one centered at 24 μm , since the sensitivity limits and background emission in MIPS channels at 70 μm and 160 μm do not allow detection of any but the brightest mid-infrared sources. The plate scale of the 24 μm

array is $2'45$; it has a spatial resolution of $6''$ (Rieke et al. 2004). The Cha I maps have a total size of about $0^{\circ}5 \times 1^{\circ}5$. The total effective exposure time per pointing at $24 \mu\text{m}$ is about 80 s. After calibration and correction for distortion, images were combined into the final mosaics within the standard post-BCD SSC pipeline. We used these archived MIPS mosaics for $24 \mu\text{m}$ flux measurements.

We considered the 157 Cha I members listed in Luhman (2004). These are mostly late-type stars with spectral classes in the range of K0–M8, including eight likely brown dwarfs with spectral types later than M6. More than 100 members of Cha I are found in the IRAC and MIPS images used in our analysis. Two small areas in the covered regions, one each for the northern and the southern field, are affected by localized extended emission associated with bright stars, overlapping PSF structures, as well as saturation effects (see Fig. 1). For objects in those areas, aperture photometry does not give reliable results. To be conservative, we excluded such objects from our analysis – 35 out of 116 in IRAC and 39 out of 126 in MIPS. We note that this excludes all stars brighter than K3. Our final list of targets contains 81 Cha I objects with spectral types that span from K3 to M8. Out of these, 69 have detectable fluxes in all four IRAC channels and in the MIPS $24 \mu\text{m}$ band. Additional 18 objects with measured $24 \mu\text{m}$ fluxes were not present in the IRAC field of view. IRAC $8 \mu\text{m}$ and MIPS $24 \mu\text{m}$ mosaics with all detected objects are presented in Fig. 1.

We performed photometry using the aperture photometry routine `aper.pro` in the IDLPHOT package. The IDLPHOT routines were integrated into a custom IDL program that uses the World Coordinate System information in the image headers to find the star within the image. The program then determines the centroid of the star and extracts the photometry. For IRAC data, we used a 5-pixel ($6''.1$) aperture for each object, with a sky annulus extending from 5 to 10 pixels for sky flux measurements. We applied an aperture correction following the instructions given in the IRAC handbook, version 3.0. For eight Cha I brown dwarfs with IRAC fluxes previously published by Luhman et al. (2005), our photometry is consistent with theirs to within the errors. For MIPS $24 \mu\text{m}$ images, we chose a $6''.6$ aperture, with a sky annulus in the range of $7\text{--}13''$. In order to account for the aperture correction, we used values tabulated in the MIPS handbook, version 3.2.1. The final list of Cha I targets with their fluxes in units of mJy measured in the 3.6 , 4.5 , 5.8 , $8 \mu\text{m}$ and $24 \mu\text{m}$ bands is given in Table I. The $J - H$ colour for all Cha I members listed in Table I is from the Two Micron All Sky Survey (2MASS) Point Source Catalog.

3. Disk Frequency

It is possible to distinguish between diskless (so-called Class III) and disk-harboring (Class II) stars using the IRAC colours, as suggested by Allen et al. (2004). The two classes of objects are indeed well separated in our IRAC colour-colour diagram (Fig. 2): diskless stars do not show colour excess in the IRAC channels and thus fall near the origin of the coordinate system, while those with disks are concentrated in a region demarcated by model colours and measured IRAC colours for objects in various other star-forming regions (Allen et al. 2004; Hartmann et al. 2005).

Another way to distinguish stars with disks from those without is to plot mid-infrared flux ratios against the $J - H$ colour, which is a reasonable proxy for the stellar photosphere. We do this in Fig. 3 for the $8\ \mu\text{m}$ to $4.5\ \mu\text{m}$ and $24\ \mu\text{m}$ to $4.5\ \mu\text{m}$ flux ratios. The presence of two populations of stars is evident. The population with lower flux ratios shows the infrared emission dominated by the stellar photospheres: these are comparable to the blackbody emission function with the temperature range that includes the effective temperatures of all Cha I members in our sample (dashed line in both panels of Fig. 3). Objects with the higher flux ratios are the ones likely to harbor circumstellar disks; dust emission from the surrounding disk contributes substantially to the infrared emission coming from these objects. Interestingly, there is a clear gap between diskless and disk-bearing stars in both panels, indicating a rapid transition between these two phases (see § 4 for further discussion).

Based on $8\ \mu\text{m}$ excess, the disk fraction among Cha I members included in our analysis is $52\% \pm 6\%$ (42/81) while for objects detected at $24\ \mu\text{m}$, it is $58^{+6}_{-7}\%$ (40/69)¹. Thus, the disk frequency we derive for Cha I is comparable to that found in the ~ 2 Myr-old IC 348 cluster ($50\% \pm 6\%$) from IRAC observations (Lada et al. 2006), but somewhat lower than the $\sim 68\%$ disk fraction reported for the ~ 1 Myr-old Taurus star-forming region, based on $3.6\ \mu\text{m}$ excess measurements (Haish et al. 2001). On the older side, only $19\% \pm 4\%$ of K+M stars in the ~ 5 Myr-old Upper Scorpius OB association show disk excess at $8\ \mu\text{m}$ and $16\ \mu\text{m}$ (Carpenter et al. 2006). A similar steep decline in the frequencies of the low-mass stars with disks is also seen in the ~ 8 Myr-old TW Hydrae association (Jayawardhana et al. 1999) and in the ~ 10 – 12 Myr old NGC 7160 cluster (Sicilia-Aguilar et al. 2006).

There have been suggestions that the disk fraction among young stars depends on spectral type and stellar mass (Lada et al. 2006; Carpenter et al. 2006; Sicilia-Aguilar et al. 2006). However, in the case of Cha I, circumstellar disks appear to be distributed evenly

¹Cautious note: Since we excluded a significant fraction of the Cha I members located close to bright stars (see § 2), our disk frequencies may be biased.

among late-type (\geq K3) stars (Fig. 4). The fraction of disk-bearing stars in our sample ranges from $47\% \pm 10\%$ for M0–M4 stars to $53^{+9}_{-10}\%$ for M4.25–M8 stars and $55^{+18}_{-19}\%$ for K3–K8 stars. These disk fractions are similar to that ($50\% \pm 17\%$) reported by Luhman et al. (2005) for very low mass objects in this region. In order to consider a possible dependence on stellar mass, we can convert the effective temperatures of Cha I members in our sample (Luhman 2004) to masses using the Baraffe et al. (1998) pre-main-sequence (PMS) evolutionary tracks for an age of ~ 2 Myr. We find that stars with masses $\gtrsim 1 M_{\odot}$ have a disk fraction of $55^{+18}_{-19}\%$ while $47\% \pm 10\%$ of those in the $0.3 M_{\odot} - \lesssim 1 M_{\odot}$ range harbor dusty disks. Again, we do not find a significant mass-dependence in the disk frequency, for Cha I members with masses of 0.1 – $1.4 M_{\odot}$. On the other hand, Lada et al. (2006) have found the highest percentage of circumstellar disks in the IC 348 cluster to be among K6–M2 stars ($\sim 56\%$), which have masses comparable to the Sun, while the disk fraction for stars $< K6$ is only $\sim 19\%$. For Upper Scorpius, the highest disk fraction is for K and M stars with masses in the 0.1 – $1 M_{\odot}$ range (Carpenter et al. 2006), although the peak value ($\sim 19\%$) is much lower than in the younger Cha I and IC 348 regions. Meanwhile, $\sim 48\%$ of G–M2 stars in Trumpler 37 (~ 4 Myr) show infrared excess (Sicilia-Aguilar et al. 2006). In summary, the evidence to date suggests that primordial disks survive for ~ 5 Myr around 20–50% of the stars with masses $\lesssim 1 M_{\odot}$, thus providing conditions for planet formation. The disk lifetime seems to be a function of object mass in some regions, but not in Cha I, thus it may also depend on the environment.

We also investigated whether there is a difference between the spatial distribution of diskless stars versus disk-bearing stars, especially in terms of their apparent distance from the two intermediate-mass stars in Cha I. The Herbig Ae/Be star HD 97048 is located in the lower cloud core, while the likely zero-age main sequence A star HD 97300 is in the upper cloud core. Figure 5 shows the positions of our targets along with those of the two early-type stars. There does not appear to be a difference between the spatial distributions of stars with $8 \mu\text{m}$ excess and those without (filled and open circles in Fig. 5, respectively), outside of $2.5'$ from HD 97300 in the upper cloud and $6'$ from HD 97048 in the lower cloud core; at smaller distances contamination from the bright stars and cloud core emission prevent reliable flux measurements (see § 2). Average positions of the two types of objects in the lower and upper cloud regions, denoted as open pentagons for disk-bearing and open squares for diskless stars, might suggest that disk-bearing objects are slightly displaced towards the central region of Cha I. However, this displacement is too small to be statistically significant. Thus, we conclude that there is no evidence for intermediate mass stars influencing disk dissipation in low-mass stars in Cha I.

4. Transition Disks

Objects that exhibit fluxes at 3–8 μm fully consistent with photospheric emission, but higher flux levels at longer wavelengths are thought to be caught in the process of inner disk clearing. These disks may have an optically thin inner region devoid of small dust grains, as in the case of CoKu Tau/4 in Taurus (D’Alessio et al. 2005). Theoretical models proposed to explain the clearing process include photoevaporation by ultraviolet radiation from the central star and grain growth related to planet formation processes (Muzerolle et al. 2006).

To identify transition disk candidates among Cha I members in our sample, we have searched for objects with no infrared colour excess at 3–8 μm (i.e., lying under the dotted line in the upper panel of Fig. 3), but with excess flux at 24 μm (i.e., lying above the dotted line in the lower panel of Fig. 3). We found two candidates: K8-type star T35 and M5-class star C7-1. We then plotted the infrared spectral energy distributions (SEDs) of these two objects, including near-infrared fluxes from the 2MASS Point Source Catalog, along with the SED of the disk-bearing star T46 (K8) for comparison (Fig. 6). All fluxes have been dereddened using A_J given in Luhman (2004) and the reddening law of Mathis (1990). All three objects show excess above the expected photospheric emission at $\lesssim 10 \mu\text{m}$ (based on the STARDUSTY 2000 models of stellar atmospheres by Allard et al. 2000), but the excess is less pronounced in T35 and C7-1. Since small ($< 10 \mu\text{m}$), warm ($T > 200 \text{ K}$) dust grains dominate emission in this wavelength region, the flatter SEDs of T35 and C7-1 may imply that their inner disks are undergoing grain growth and dust settling to the optically thick midplane (Scholz et al. 2007). However, their inner disks are not completely devoid of small grains, unlike the case in previously studied transition objects (e.g., D’Alessio et al. 2005; Muzerolle et al. 2006).

5. Connections with Accretion and Binarity

Our Cha I sample is ideally suited for investigating the effects of stellar properties and immediate environment on disk dissipation, because high-resolution optical spectra and high-angular resolution images are available for a substantial fraction of the targets. The optical spectra, obtained with MIKE on the Magellan/Clay 6.5 m telescope, include tracers of disk accretion for 35 objects (Nguyen et al., in prep.; Mohanty et al. 2005; Muzerolle et al. 2005). Adaptive optics (AO) imaging with NACO on the ESO Very Large Telescope has been carried out for 65 of our targets (Ahmic et al., in prep.).

5.1. Accretion

The strength of the $H\alpha$ emission line is widely used as a signature of (gas) accretion from a disk onto the central star (e.g., Jayawardhana et al. 2006). In the spectra of accreting objects, the line is dominated by emission produced in the infalling gas, whereas in non-accretors the line is weaker because it comes only from chromospheric activity. Traditionally, young stars were classified as either classical T Tauri stars (CTTS) if the $H\alpha$ equivalent width (EW) is $> 10 \text{ \AA}$ or as weak-line T Tauri stars (WTTS) if the $\text{EW} < 10 \text{ \AA}$. But, since the EW depends on the spectral type, White & Basri (2003) proposed the full width of the line at 10% of the peak as a more robust accretion diagnostic. Based on empirical and physical arguments, Jayawardhana et al. (2003) adopted an $H\alpha$ 10% width of $\sim 200 \text{ km s}^{-1}$ as a dividing line between accretors and non-accretors, to be applicable to the very low mass regime as well. In fact, Natta et al. (2004) have found that the $H\alpha$ 10% correlates well with the mass accretion rate derived in other ways, and that the $\sim 200 \text{ km s}^{-1}$ threshold corresponds to the mass accretion rate $\sim 10^{-11} \text{ M}_{\odot} \text{ yr}^{-1}$.

To examine the connection between dusty inner disks and gas accretion, in Fig. 7 we show the $8 \mu\text{m}$ excess versus $H\alpha$ 10% widths for those Cha I members for which both measurements are available. (The error bars on the $H\alpha$ 10% width refer to the standard deviations of the estimates over four epochs of observations.) Out of 35 objects in this sub-sample, 14 do not show evidence of accretion or dust emission (cf. lower left region in Fig. 7), implying that their inner disks have probably been cleared of both dust and gas. Of 21 objects with infrared excess, 15 appear to be accreting.² Thus, in the vast majority of cases (29/35) the signature of accretion is well correlated with evidence of a dusty disk. This finding suggests that, on average, the gas dissipation timescale is comparable to the timescale for clearing the inner disk of small dust grains.

However, six out of the 21 disk-bearing objects in this sub-sample lie below the accretion threshold (upper left part of Fig. 7). Five out of these six objects are in the low-mass regime, with the masses $\lesssim 0.3 \text{ M}_{\odot}$ (see Table 2). One possible explanation is that accretion rates have dropped below measurable levels even though dust disks persist in these cases. Another explanation is variable accretion: it may well be the case that quiescent phases dominate in the latest stages of accretion, so some objects with disks are observed during the non-accreting epochs (see Hartmann et al. 2005; Lada et al. 2006; Sicilia-Aguilar et al. 2006; Scholz et al. 2007).

²For two of the objects –CHX 18N and T35– the $8 \mu\text{m}$ excess is relatively weak; the latter does have substantial excess at $24 \mu\text{m}$ (see § 4) while for the former we could not measure it reliably due to background contamination.

5.2. Binarity

Theoretical models of the evolution of T Tauri disks in binary systems show that the individual circumstellar disks are truncated due to tidal effects. Once truncated, the two disks evolve independently, unless gap-clearing and circumbinary disk formation occur (Lubow & Artymowicz 1996).

Of the Cha I members in our sample, 65 have also been imaged with AO on the ESO VLT (Ahmic et al., in prep.). Among them, there are 15 binaries and two triple systems. In Fig. 8, we show the $8/4.5\ \mu\text{m}$ flux ratio against projected binary separation for this subsample. Given the relatively poor angular resolution of IRAC and MIPS (§ 2), these multiple systems are unresolved in the *Spitzer* images; thus, we cannot determine which companion is responsible for the infrared excess. Nine of the binaries do not show infrared excess, while other six appear to harbor disks based on the $8/4.5\ \mu\text{m}$ flux ratio. Neither of the two triples shows mid-infrared excess.

The projected separations of the AO-resolved binaries range from ~ 10 AU to ~ 300 AU. Of the five binaries with $\lesssim 20$ AU separations, four –including the two closest pairs– exhibit low $8/4.5\ \mu\text{m}$ flux ratios typical for diskless objects. This implies that either the disks have dissipated completely or a large inner hole is carved out by the companion; in the latter scenario, the disk would be circumbinary and undetectable with the near- and mid-IR data used in our analysis. The closest pair with detectable disk excess –Hn 13– is separated by ~ 20 AU. Theoretical modeling suggests that tidally truncated disks would have outer radii between 0.3–0.4 times the physical separation between the two stars for binaries with mass ratios close to one (Papaloizou & Pringle 1977). Thus, the disk(s) in the Hn 13 binary system would have an outer radius of ~ 8 AU: emission from dust within this radius may explain the excess at 8 and $24\ \mu\text{m}$.

The two triple systems detected, CHXR 28 and T39, do not exhibit $8\ \mu\text{m}$ or $24\ \mu\text{m}$ excess. Their projected separations are 24, ~ 290 AU and ~ 200 , ~ 720 AU, respectively. Again, the lack of mid-infrared excess may indicate faster disk dissipation due to the presence of companions or growth of large inner holes.

In a recent study of the $\simeq 8$ Myr old η Chamaeleontis star cluster, Bouwman et al. (2006) reported that disks clear out more rapidly in binary systems with projected separations $\lesssim 20$ AU. Their analysis of 15 K- and M-type stars, using their own *Spitzer* observations and AO-imaging by Brandeker et al. (2006), shows that only one out of six binaries ($17_{-14}^{+28}\%$) retains a dusty disk while eight out of nine single stars ($89_{-21}^{+9}\%$) harbor disks. Thus, they concluded that circumstellar disks and binarity are anti-correlated. We also find that the disk excess fraction is lower among multiple systems ($35_{-13}^{+15}\%$) than among (apparently) single

stars ($48\% \pm 8\%$) in Cha I, but the difference is less pronounced in this (younger) region. (The disk frequency for the total sample of 65 objects is $45\% \pm 7\%$, a value slightly higher than that for multiple systems.) If we consider only those binaries with $\lesssim 20$ AU separations, 4/5 do lack infrared excess. It may be that companions at (projected) distances $\gtrsim 20$ AU do not have a strong effect on inner disk dissipation (at least not within $\simeq 2$ Myr).

6. Summary

We have presented a comprehensive view on the disks around stars and brown dwarfs in the nearby, young Cha I dark cloud. In the following, we summarize our results:

1. We used archival *Spitzer* data to measure mid-infrared fluxes in the wavelength range 3–24 μm for 81 known members of the Cha I star forming region. Our sample shows a clear bimodality in their *Spitzer* colours (flux ratios 8/4.5 μm and 24/4.5 μm). For about half of the objects, the mid-infrared colours are consistent with purely photospheric emission, while the other half shows substantial mid-infrared colour excess, interpreted as emission from a dusty disk. In both colours, there is a clear gap between the two groups of objects.
2. The overall disk frequency in our sample is $52\% \pm 6\%$ based on the 8/4.5 μm colour and $58^{+6}_{-7}\%$ based on the 24/4.5 μm colour. This value is consistent with the disk fractions found in similarly aged regions like IC 348 and Taurus (Haish et al. 2001; Hartmann et al. 2005; Lada et al. 2006). In contrast, the stellar disk frequency in the somewhat older star forming region Upper Scorpius (age ~ 5 Myr) appears to be significantly lower ($\sim 20\%$, Carpenter et al. 2006).
3. The disk fraction in our sample is, within the statistical uncertainties, not a function of spectral type: independent of the chosen binning, it ranges between 47% and 55% for spectral types between K3 and M8. This is in contrast to recent findings in other star forming regions, where the disk frequency has been found to change significantly in the same spectral range (Lada et al. 2006; Carpenter et al. 2006; Scholz et al. 2007). Environmental differences and mass-dependent disk evolution might be important aspects to explain these findings.
4. There is no clear difference in the spatial distribution of stars with and without disks. The presence of bright stars in Cha I does not seem to have any effect on the spatial distribution of dusty disks at distances greater than few arcmin. Although average positions of stars with disks within the two Cha I cores are slightly displaced with

respect to the average positions of disk-bearing stars, the difference is too small to be statistically important.

5. In our sample, there are no definitive transition disks, i.e. objects without excess at 3–8 μm , but significant excess at longer wavelengths. These transition disks are often discussed as objects caught in the process of inner disk clearing. However, we find two objects which have weak excess emission at 3–8 μm (and no colour excess at these wavelengths), but substantial excess at 24 μm . These objects may be potential precursors to transition disks. This type of SED is best seen in the late-K type star T35, which shows a rising SED at 24 μm .
6. For 35 objects in our sample, we combined the *Spitzer* data with results from high-resolution optical spectroscopy. As a proxy for accretion, we use the H α 10% width and adopt a threshold of 200 km s $^{-1}$ between accretors and non-accretors. Among the vast majority (29/35), there is a correlation between accretion signatures and infrared excess, consistent with the idea that the dust clearing of the inner disk coincides with a cessation of the gas accretion. However, six of the non-accretors still show signs of an inner dust disk. Thus, in some cases young objects can retain their disks, after continuous accretion has stopped or at least dropped below measurable levels.
7. We use the results from a Cha I imaging survey with high spatial resolution using the AO system NACO at ESO/VLT to investigate the impact of multiplicity on the disk properties. AO images have been obtained for 65 objects in our *Spitzer* sample, 17 of them have companions at separations between 0''.06 and 5'', corresponding to (projected) physical separations of 10–800 AU. The disk frequency among the objects with companions ($35^{+15}_{-13}\%$) is lower than (but still consistent with) the value for the total sample, which might hint that the presence of a companion contributes to faster disk dispersal. However, the existence of six objects with disks and companions (at separations between 20–300 AU) suggests that the dispersion of the inner disk is not strongly affected by companions at $\gtrsim 20$ AU. For the closest binary with disk, the companion sets an upper limit for the outer disk radius of ~ 8 AU. (Note that all multiple systems are unresolved in *Spitzer* images, implying that we cannot determine which component is responsible for the mid-infrared excess.)

This research was supported by NSERC grants to RJ and MHvK, and an Early Researcher Award from the Province of Ontario to RJ.

REFERENCES

- Allard, F, Hauschildt, P. H., & Schwenke D. 2000, ApJ, 540, 1005
- Allen, L. E., Calvet, N., D’Alessio, P., et al. 2004, ApJS, 154, 363
- André, P., Ward-Thompson, D., & Barsony, M. 2000, in Mannings, v., Boss, A. P., & Russell, S. S., eds, Protostars and Planets IV, Tuscon: Univ. Arizona Press, p.59
- Baraffe, I., Chabrier, G., Allard, F., & Hauschildt, P. H. 1998, A&A, 337, 403B
- Bouwman, J., Lawson, A., Dominik, C., et al. 2006, ApJ, 653, L57
- Brandeker, A., Jayawardhana, R., Khavari, P., et al. 2006, ApJ, 652, 1572
- Calvet, N., D’Alessio, P., Watson, P. D., et al. 2005, ApJ, 630, L185
- Carpenter, J. M., Mamajek, E. E., Hillenbrand, L. A., & Meyer, M .R. 2006, ApJ, 651, L49
- D’Alessio, P., Hartmann, L., Calvet, N., et al. 2005, ApJ, 621, 461
- Fazio, G. G., et al. 2004, ApJS, 154, 10
- Haish, H. E., Lada, E. A., & Lada, C. J. 2001, ApJ, 533, L153
- Hartmann, L., Megeath, S. T., Allen, L., et al. 2005, ApJ, 629, 881
- Jayawardhana, R., Hartmann, L., Fazio, G., et al. 1999, ApJ, 521, L129
- Jayawardhana, R., Mohanty, S., & Basri, G. 2003, ApJ, 592, 282
- Jayawardhana, R., Coffey, J. Scholz, A., et al. 2006, ApJ, 648, 1206
- Lada, C. J., Muench, A. A., Luhman, K. L., et al. 2006, ApJ, 131, 1574
- López Martí, B., Eislöffel, J., Scholz, A., & Mundt, R. 2004, A&A, 416, 555
- Lubow, S. H. & Artymowicz, P. 1996, in Wijers, R. A. M. J., Davies, M. B., & Tout, C. A., eds, Evolutionary Processes in Binary Stars. Kluwer Academic Publishers, p.53
- Luhman, K. L. 2004, ApJ, 602, 816
- Luhman, K. L., D’Alessio, P., Calvet, N., et al. 2005, ApJ, 620, L516
- Mathis, J. S. 1990, ARA&A, 28, 37
- Mohanty, S., Jayawardhana, R., & Basri, G. 2005, ApJ, 626, 498

- Muzerolle, J., Luhman, k. L., Briceño, C., et al. 2005, ApJ, 625, 906
- Muzerolle, J., Adame, L., D’alessio, P., et al 2006, ApJ, 643, 1003
- Natta, A., Testi, L., Muzerille, J., et al. 2004, A&A, 424, 603
- Papaloizou, J. & Pringle, J. E. 1997, MNRAS, 181, 441
- Rieke, G. H., et al. 2004, ApJS, 154, 25
- Scholz, A., Jayawardhana, R., Wood, K., et al. 2007, ApJ, 660, 1517
- Sicilia-Aguilar, A., Hartmann, L., Calvet, N. et al. 2006, ApJ, 638, 897
- White, R. J., & Basri, G. 2003, ApJ, 582, 1109
- Whittet, D. C. B., Prusti, T., Franco, G. A. P., et al. 1997, A&A, 327, 1194

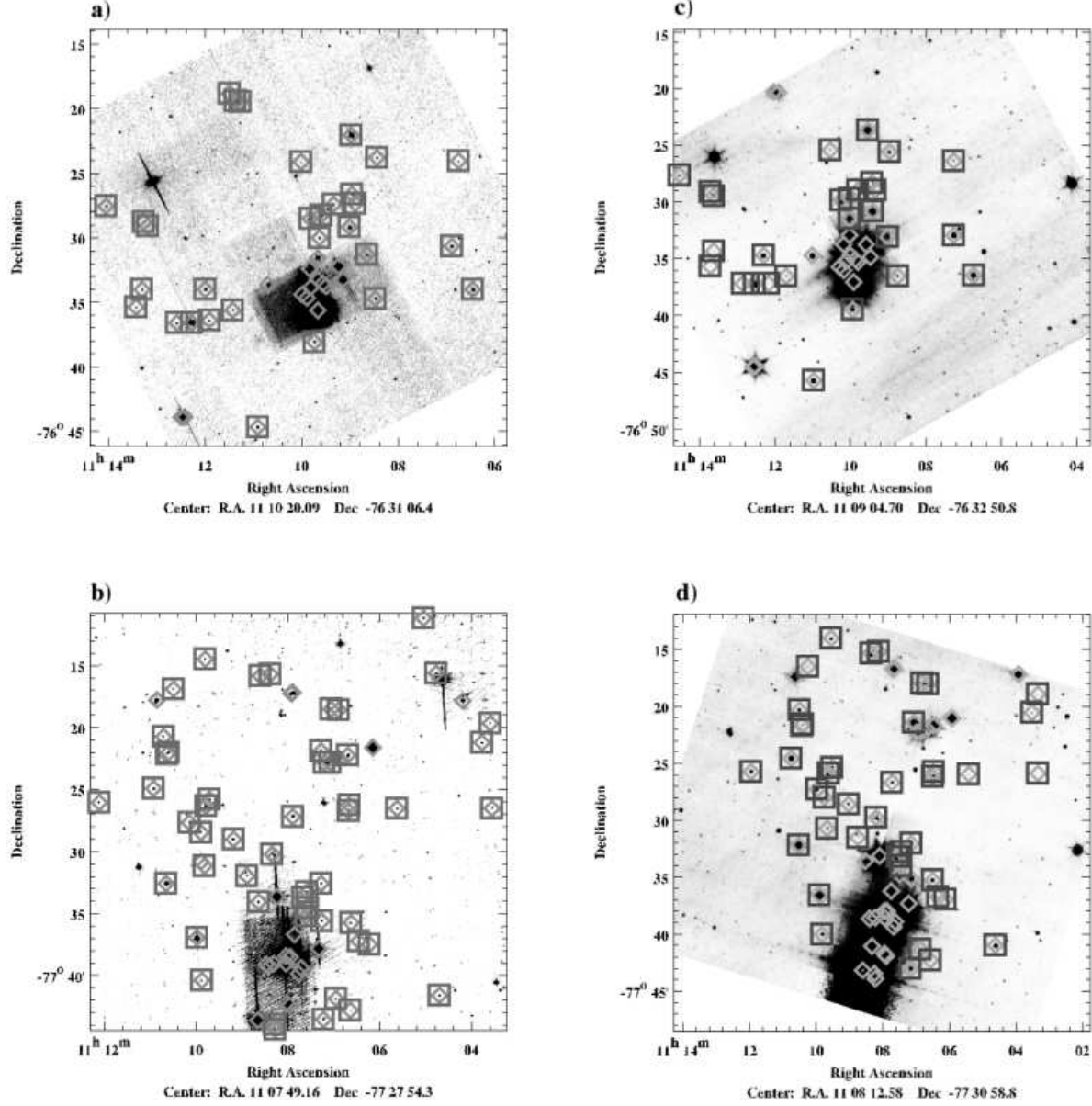


Fig. 1.— IRAC 8 μm and MIPS 24 μm mosaics with the positions of all detected Cha I members denoted with *diamonds* and positions of the objects used in our analysis presented with *squares*; a) upper cloud core mosaic in 8 μm band, b) lower cloud core mosaic in 8 μm band, c) upper cloud core mosaic in 24 μm band, d) lower cloud core mosaic in 24 μm band.

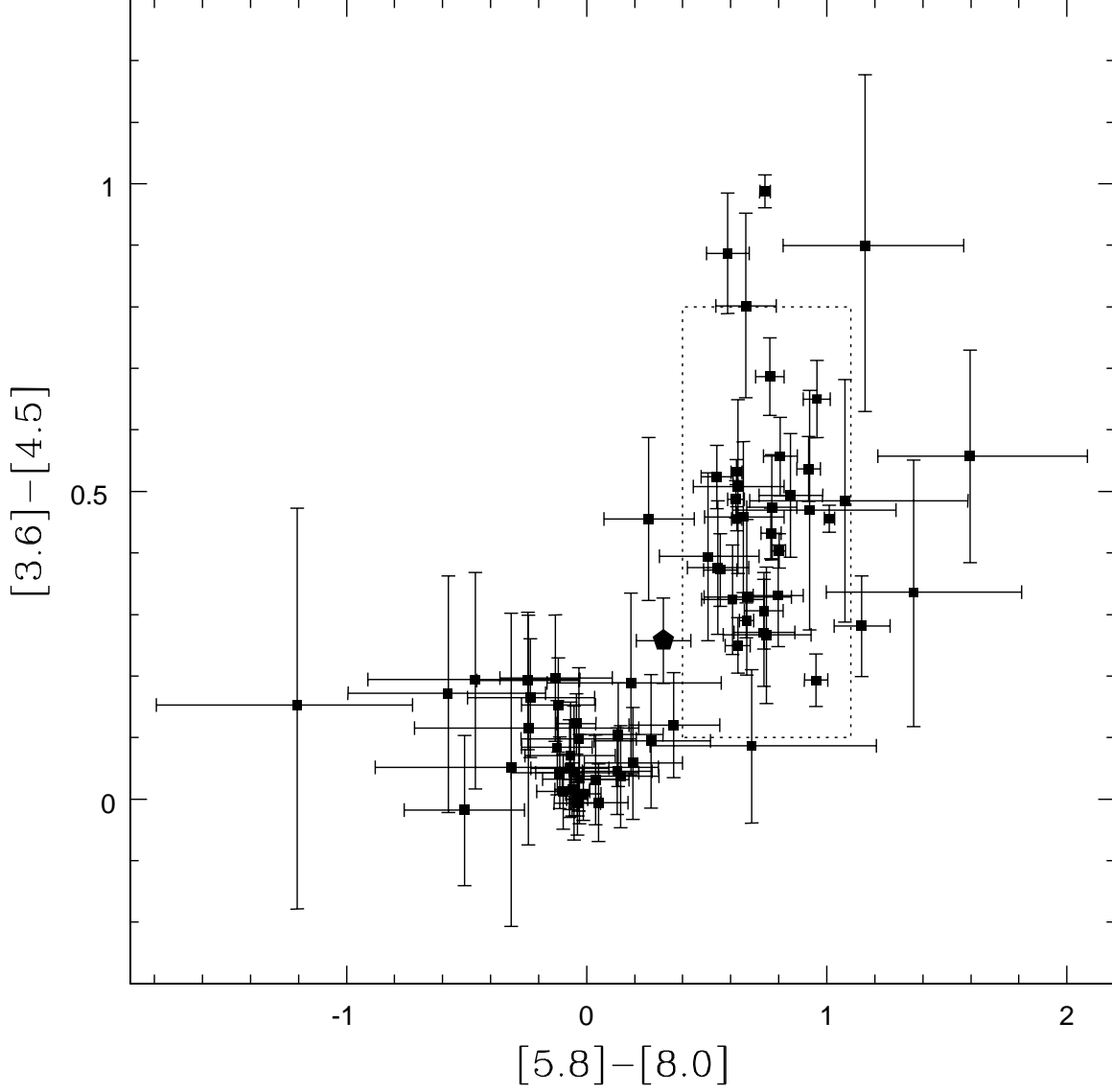


Fig. 2.— IRAC colour-colour diagram for 71 objects in Cha I star-forming region. The *dotted square* denotes the domain of objects with circumstellar disks (Allen et al. 2004; Hartmann et al. 2005). Objects without disk excess are located near the origin of the coordinate system. One transition object candidate –C7-1– with measured fluxes in all four IRAC channels is presented with *pentagon*.

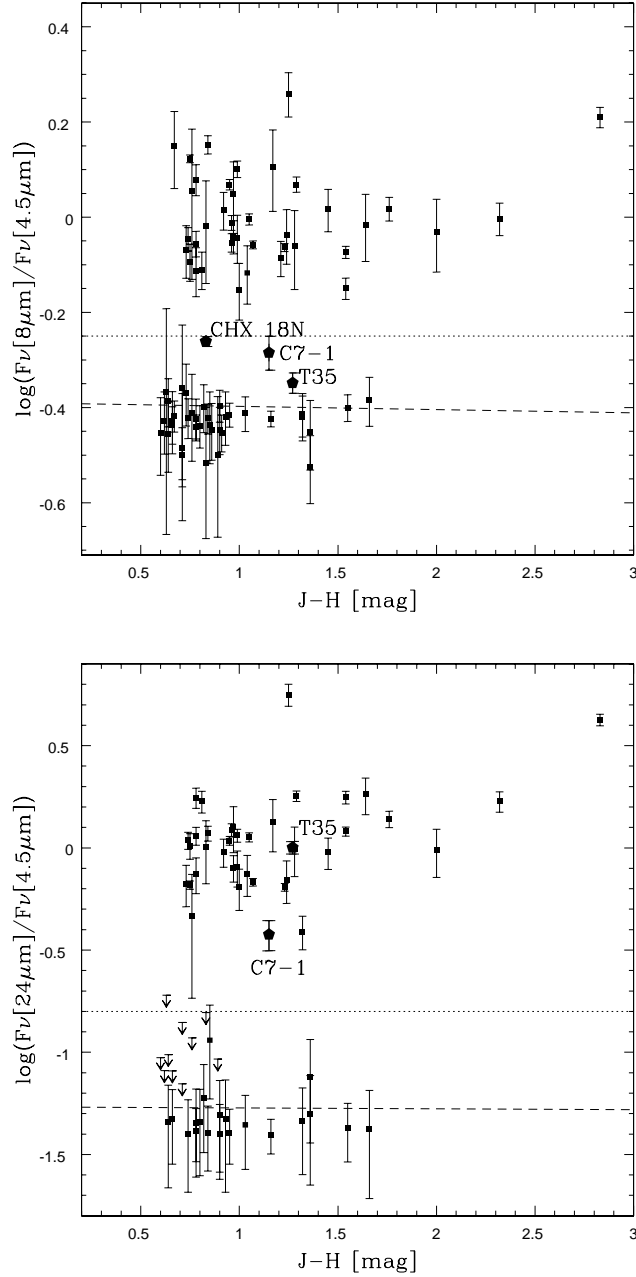


Fig. 3.— Colour-colour diagrams with circumstellar disks tracers ($8\,\mu\text{m}$ to $4.5\,\mu\text{m}$ flux ratio in the top panel and $24\,\mu\text{m}$ to $4.5\,\mu\text{m}$ ratio in the bottom panel) vs. a stellar photosphere tracer ($J - H$). Arrows in the lower panel represent objects for which only upper limits for $24\,\mu\text{m}$ fluxes could be estimated. *Dashed line* in both panels corresponds to the photospheric $8\,\mu\text{m}$ to $4.5\,\mu\text{m}$ flux ratio. The *dotted lines* represent conservative thresholds for circumstellar disk presence, in our case a 40% excess above the photosphere in the $8/4.5\,\mu\text{m}$ and $24/4.5\,\mu\text{m}$ flux ratios. There are two objects that appear to lie under the threshold in the top panel, but occupy the region above the threshold in the bottom one. These are candidates for the transition objects, i.e. stars with possible clearings in their disks. A third object from the upper panel –CHX 18N– does not have $24\,\mu\text{m}$ flux measured. All three object are presented with *pentagons* and labeled.

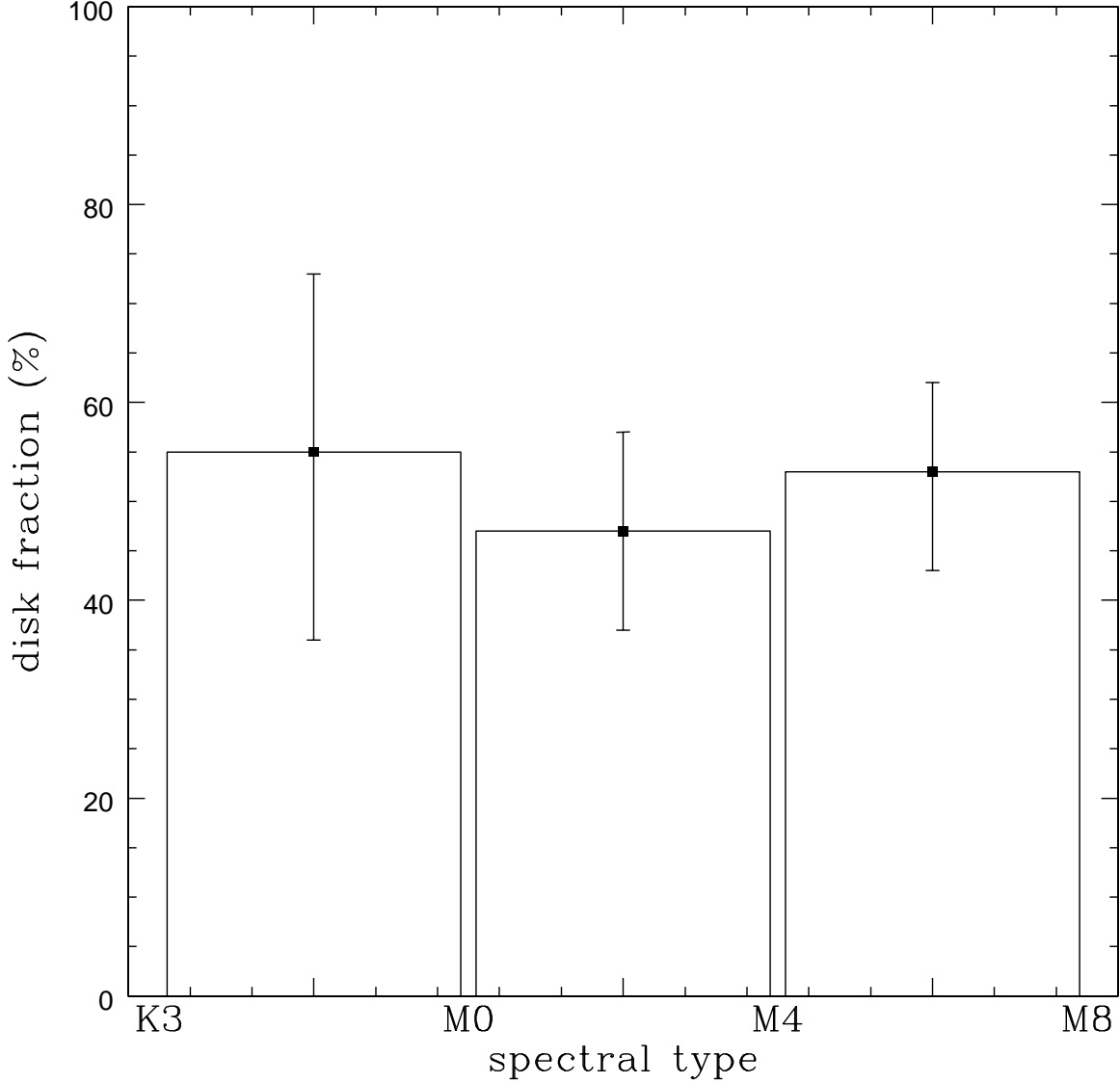


Fig. 4.— Histogram of the disk fraction as a function of spectral type for Cha I members. The spectral type information is taken from Luhman (2004) while the disk detection is based on the $8\ \mu\text{m}$ excess. The majority of stars in Cha I and all objects included in this study are of spectral types later than K3. In order to have roughly the same number of objects in every bin, we divided our sample into three bins. The obtained distribution shows that there is no significant difference between the disk fractions among stars of different (late) spectral types in Cha I.

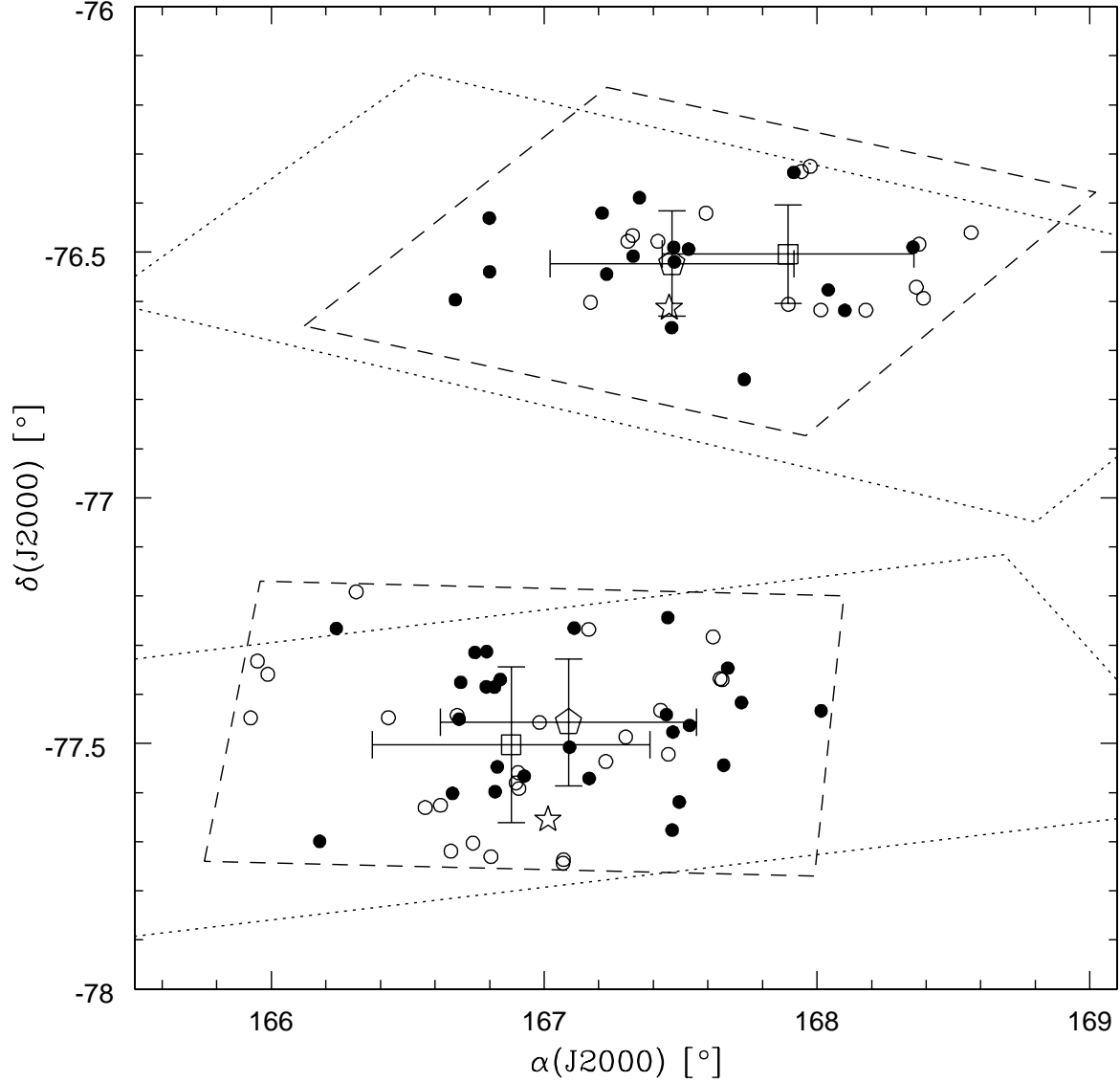


Fig. 5.— Spatial distribution of Cha I members: *filled circles* correspond to the positions of the disk bearing objects, while objects without any infrared excess due to disk presence are denoted with *open circles*. The two *stars* represent intermediate mass stars - HD 97048 in the lower cloud core and HD 97300 in the upper one. *Open squares* and *open pentagons* mark the average positions of diskless and disk-bearing stars, respectively, in the two cores. *Dashed lines* correspond to the boundaries of IRAC maps, and *dotted lines* correspond to the boundaries of the 24 μm MIPS maps.

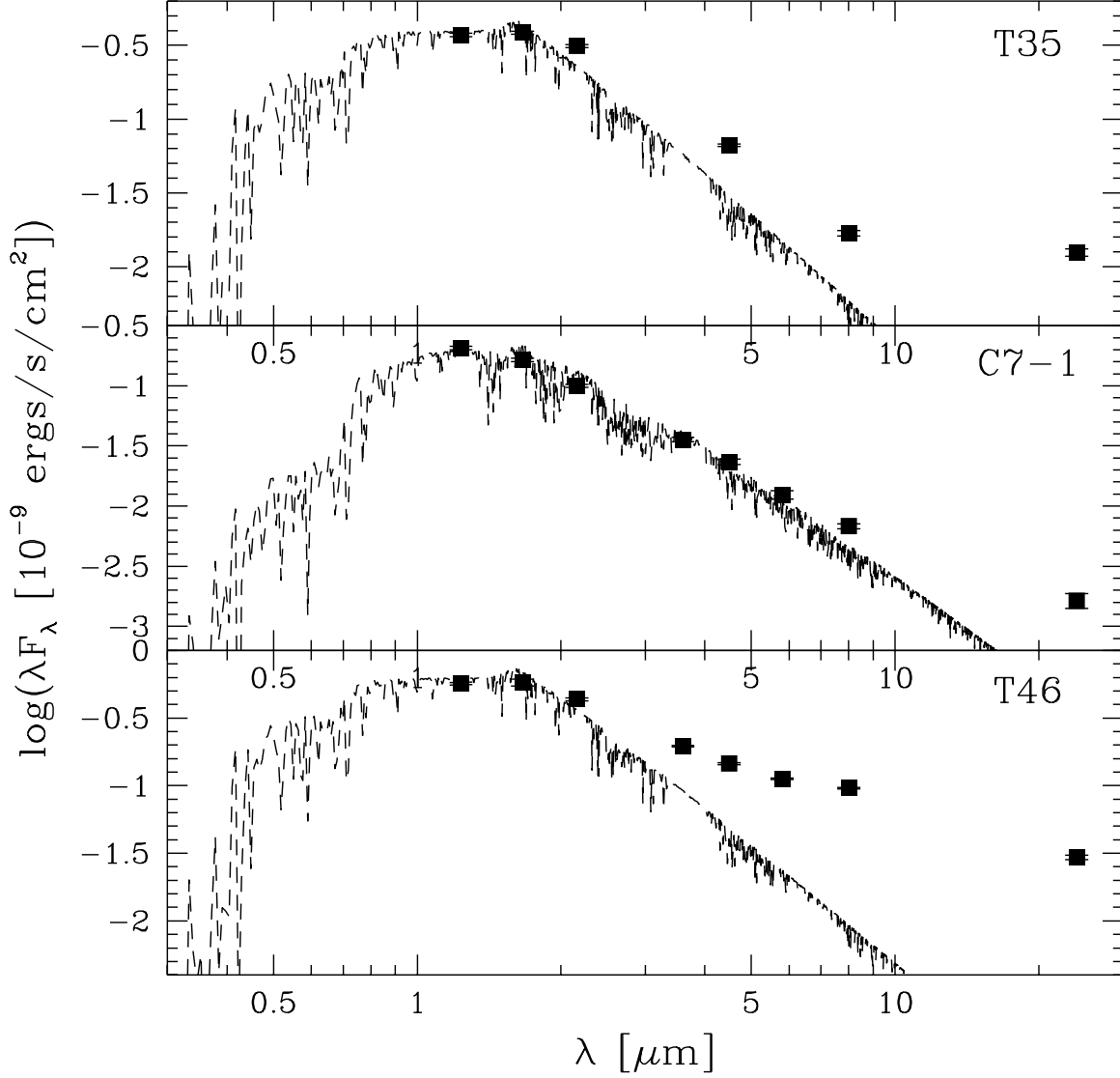


Fig. 6.— SEDs for two transition object candidates (T35 and C7-1) and one typical disk-bearing Cha I member (T46). In each panel measured fluxes in 2MASS, IRAC and 24 μm MIPS bands are presented with *squares*; the model stellar photosphere corresponding to the object’s effective temperature (STARDUSTY2000, Allard et al. 2000) is shown with the *dashed line* for comparison.

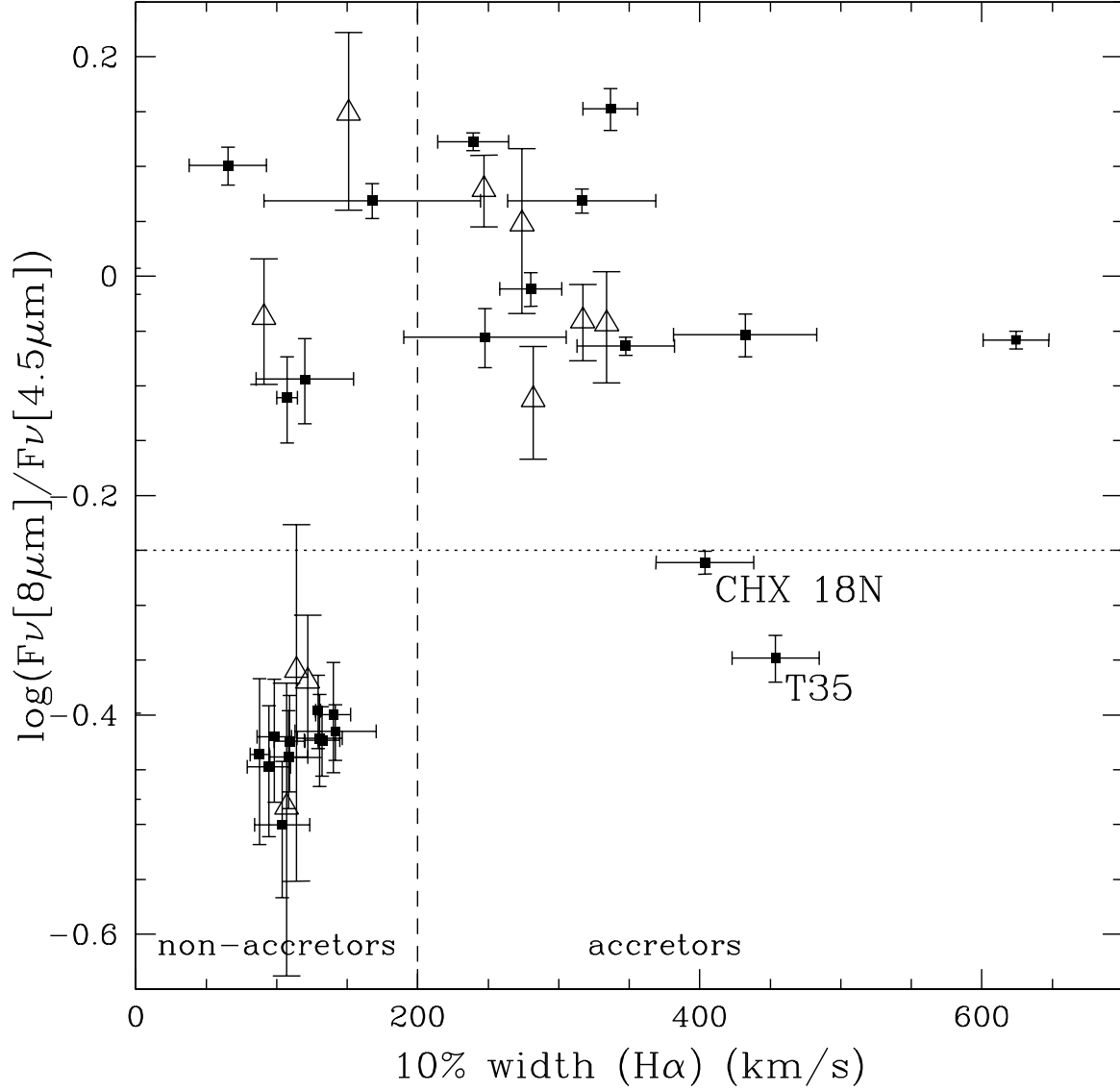


Fig. 7.— $8\mu\text{m}$ excess vs. the full width of $\text{H}\alpha$ line at 10% of the peak for 35 Cha I members. The $\text{H}\alpha$ widths are taken from Nguyen et al. (in prep.; *filled squares*), Mohanty et al. (2005) and Muzerolle et al. (2005) (*open triangles*). The *dashed line* corresponds to the accretion cutoff adopted by Jayawardhana et al. (2003). The threshold for disk presence on the basis of IRAC colour excess is represented by *dotted line* as in the upper panel of Fig. 3. The two objects with prominent accretion signatures and yet without colour excess at $8/4.5\mu\text{m}$ are labeled.

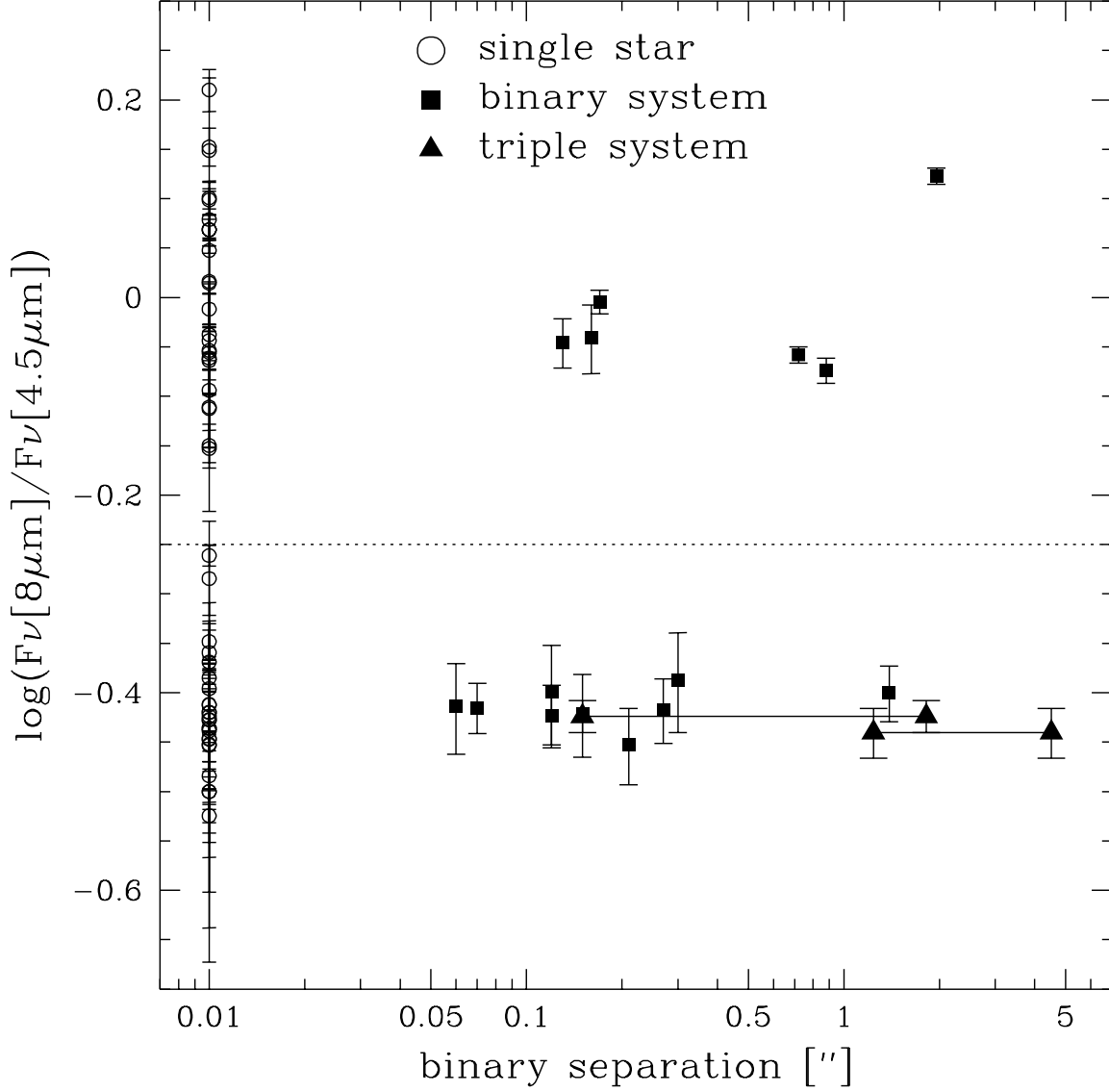


Fig. 8.— 8 μm excess, indicating presence of a disk, vs. binary separation for 65 Cha I members (from Ahmic et al., in prep.). The *dotted line* represents the threshold for 8 μm excess from a circumstellar disk, taken from the upper panel of Fig. 3. Two triple systems are presented with both separation values connected by *solid lines*. Single objects are positioned at the binary separation of 0".01 for presentation purposes only.

Table 1. Chamaeleon I members with detectable infrared fluxes

ID	SpT ^a	$J-H^b$ (mag)	3.6 μm^c	4.5 μm^c	5.8 μm^c	8 μm^c	24 μm^d
			(mJy)				
ISO 28.....	M5.5	0.89	9.1 \pm 0.7	6.5 \pm 0.7	4.6 \pm 0.9	2.0 \pm 0.5	0.6 ^e
Hn 2.....	M5	0.90	37 \pm 2	25 \pm 1	17 \pm 2	8.9 \pm 0.7	1.2 \pm 0.6
CHXR 12.....	M3.5	0.80	45 \pm 2	30 \pm 2	20 \pm 2	10.9 \pm 0.7	1.4 \pm 0.6
ISO 52.....	M4	0.81	29 \pm 1	24 \pm 1	17 \pm 2	18.4 \pm 0.9	40 \pm 4
T16.....	M3	1.21	...	26 \pm 1	...	21 \pm 1	...
Hn 4.....	M3.25	0.91	...	39 \pm 2	...	13.8 \pm 0.8	...
CHXR 15.....	M5.25	0.64	33 \pm 2	24 \pm 1	12 \pm 2	9.7 \pm 0.7	1.1 \pm 0.5
Cam2-19.....	M2.75	1.66	35 \pm 2	23 \pm 1	15 \pm 1	9.6 \pm 0.8	1.0 \pm 0.5
CHXR 73.....	M3.25	1.36	22 \pm 1	14.5 \pm 0.8	10 \pm 2	5.1 \pm 0.6	1.1 \pm 0.5
Cha H α 12.....	M6.5	0.71	8.6 \pm 0.7	6.4 \pm 0.7	6 \pm 2	2.1 \pm 0.5	0.9 ^e
ISO 79.....	M5.25	1.64	8.3 \pm 0.7	8.9 \pm 0.8	4 \pm 1	8.5 \pm 0.7	16 \pm 2
Hn 5.....	M4.5	0.84	63 \pm 2	66 \pm 2	71 \pm 2	94 \pm 2	77 \pm 5
T22.....	M3	1.03	65 \pm 2	42 \pm 2	32 \pm 2	16.3 \pm 0.9	1.9 \pm 0.7
CHXR 20.....	K6	0.99	113 \pm 2	86 \pm 2	81 \pm 3	109 \pm 2	99 \pm 6
Ced 110-IRS 4.....	19 \pm 1	28 \pm 2	30 \pm 2	29 \pm 1	...
CHXR 74.....	M3	0.93	30 \pm 2	20 \pm 1	12 \pm 2	7.7 \pm 0.7	1.0 \pm 0.5
T23.....	M1.5	0.78	32 \pm 2	27 \pm 1	20 \pm 2	32 \pm 2	47 \pm 4
Ced 110-IRS 6.....	197 \pm 3	314 \pm 4	356 \pm 4	394 \pm 4	...
ISO 91.....	M2.5	2.32	27 \pm 1	27 \pm 1	23 \pm 2	27 \pm 1	45 \pm 4
CHSM 9484.....	M5.25	0.76	5.6 \pm 0.6	2.7 \pm 0.5	...	3.0 \pm 0.6	1.2 \pm 0.6
T24.....	M0.5	0.96	98 \pm 2	79 \pm 2	70 \pm 2	70 \pm 2	96 \pm 5
CHXR 22E.....	M3.5	1.32	40 \pm 2	28 \pm 1	21 \pm 2	10.6 \pm 0.8	11 \pm 2
ISO 97.....	M1	...	42 \pm 2	51 \pm 2	57 \pm 2	64 \pm 2	...
Cha H α 1.....	M7.75	0.67	6.7 \pm 0.7	5.8 \pm 0.7	4 \pm 2	8.2 \pm 0.7	...
Cha H α 9.....	M5.5	1.24	11.8 \pm 0.8	12.0 \pm 0.8	11 \pm 2	11.0 \pm 0.8	8 \pm 2
B35.....	M2	2.83	43 \pm 2	51 \pm 2	61 \pm 2	82 \pm 2	214 \pm 8
CHXR 76.....	M4.25	0.85	16.7 \pm 0.9	11.6 \pm 0.8	4 \pm 2	4.2 \pm 0.5	1.3 \pm 0.6
CHXR 26.....	M3.5	1.55	89 \pm 2	63 \pm 2	47 \pm 2	25 \pm 1	2.7 \pm 0.8
Cha H α 7.....	M7.75	0.71	5.5 \pm 0.6	3.7 \pm 0.5	4 \pm 2	1.6 \pm 0.4	...
Cha H α 2.....	M5.25	0.97	30 \pm 1	26 \pm 1	20 \pm 2	24 \pm 1	21 \pm 3
CHXR 28.....	K6	1.16	290 \pm 4	186 \pm 3	130 \pm 3	70 \pm 2	7 \pm 2
T34.....	M3.75	0.86	34 \pm 2	23 \pm 1	16 \pm 2	8.3 \pm 0.8	...
Cha H α 13.....	M5.5	0.73	22 \pm 1	15.6 \pm 0.9	9 \pm 2	6.7 \pm 0.7	...
ISO 143.....	M5	0.92	20 \pm 1	20 \pm 1	17 \pm 2	21 \pm 1	19 \pm 3
ISO 147.....	M5.75	0.83	...	5.0 \pm 0.7	...	4.8 \pm 0.6	5 \pm 1
T35.....	K8	1.27	...	100 \pm 2	...	45 \pm 2	101 \pm 6
Cha H α 6.....	M5.75	0.78	19 \pm 1	15.9 \pm 0.9	11 \pm 2	12.3 \pm 0.8	12 \pm 2
CHXR 33.....	M0	0.90	67 \pm 2	45 \pm 2	36 \pm 2	17.9 \pm 0.9	1.8 \pm 0.7
T37.....	M5.25	0.73	15.1 \pm 0.8	13.1 \pm 0.9	11 \pm 2	11.1 \pm 0.7	9 \pm 2
CHXR 78C.....	M5.25	0.76	13.4 \pm 0.8	10.2 \pm 0.8	6 \pm 2	4.0 \pm 0.6	1.2 ^e
ISO 165.....	M5.5	1.00	13.8 \pm 0.9	13.4 \pm 0.9	13 \pm 2	9.4 \pm 0.7	9 \pm 2
T39.....	M2	0.78	124 \pm 3	80 \pm 2	53 \pm 2	29 \pm 1	3.3 \pm 0.9
CHXR 35.....	M4.75	0.64	17.6 \pm 0.9	12.3 \pm 0.8	8.0 \pm 0.9	4.3 \pm 0.5	1.2 ^e
CHXR 37.....	K7	0.95	118 \pm 2	77 \pm 2	56 \pm 2	29 \pm 1	3.1 \pm 0.9
CHXR 79.....	M1.25	1.54	191 \pm 3	191 \pm 3	163 \pm 3	161 \pm 3	230 \pm 9
T40.....	K6	1.23	406 \pm 4	424 \pm 4	370 \pm 4	366 \pm 4	272 \pm 10
CHXR 40.....	M1.25	0.84	87 \pm 2	55 \pm 2	39 \pm 2	21 \pm 1	2.2 \pm 0.8
C7-1.....	M5	1.15	43 \pm 2	35 \pm 2	24 \pm 2	18.1 \pm 0.9	13 \pm 2
B43.....	M3.25	1.54	67 \pm 2	69 \pm 2	53 \pm 2	49 \pm 2	123 \pm 6
ISO 209.....	M1	2.0	...	7.8 \pm 0.7	...	7.3 \pm 0.7	8 \pm 2
KG 102.....	M5.5	0.83	10.0 \pm 0.7	7.7 \pm 0.7	6 \pm 2	2.3 \pm 0.5	1.2 ^e
ISO 217.....	M6.25	0.99	15.3 \pm 0.8	14.9 \pm 0.9	13 \pm 2	13.5 \pm 0.8	12 \pm 2
CHSM 15991.....	M3	1.17	4.0 \pm 0.6	5.9 \pm 0.7	5 \pm 2	7.5 \pm 0.7	8 \pm 2
ISO 220.....	M5.75	1.28	7.5 \pm 0.7	7.4 \pm 0.7	5 \pm 1	6.4 \pm 0.7	7 \pm 2
T43.....	M2	1.29	109 \pm 2	103 \pm 2	107 \pm 3	121 \pm 3	185 \pm 8
ISO 225.....	M1.75	1.25	9.0 \pm 0.7	12.0 \pm 0.8	21 \pm 2	22 \pm 1	68 \pm 5
T45.....	K8	1.07	458 \pm 5	446 \pm 4	393 \pm 4	390 \pm 4	303 \pm 11
T46.....	K8	0.95	235 \pm 3	218 \pm 3	218 \pm 3	255 \pm 3	236 \pm 9
ISO 235.....	M5.5	1.45	18.9 \pm 0.9	17.1 \pm 0.9	19 \pm 2	17.7 \pm 0.9	16 \pm 2
CHSM 17173.....	M8	0.63	4.3 \pm 0.6	3.2 \pm 0.6	7 \pm 1	1.4 \pm 0.5	0.6 ^e
Hn 12W.....	M5.5	0.62	...	14.8 \pm 0.9	...	5.5 \pm 0.6	1.2 ^e
2MASS 11103481-7722053	M4	1.32	40 \pm 2	30 \pm 2	23 \pm 2	11.3 \pm 0.8	1.4 \pm 0.6
ISO 250.....	M4.75	1.36	26 \pm 1	20 \pm 1	13 \pm 2	5.9 \pm 0.7	1.0 \pm 0.5
CHXR 47.....	K3	1.05	241 \pm 3	201 \pm 3	193 \pm 3	199 \pm 3	227 \pm 9
ISO 252.....	M6	0.97	7.0 \pm 0.7	7.0 \pm 0.7	5 \pm 2	7.8 \pm 0.7	9 \pm 2
ISO 256.....	M4.5	1.76	45 \pm 2	48 \pm 2	42 \pm 2	50 \pm 2	66 \pm 5

Table 1—Continued

ID	SpT ^a	$J-H^b$ (mag)	3.6 μm^c	4.5 μm^c	5.8 μm^c (mJy)	8 μm^c	24 μm^d
Hn 13	M5.75	0.74	56 ± 2	50 ± 2	48 ± 2	45 ± 2	54 ± 4
CHXR 48 . . .	M2.5	0.78	45 ± 2	29 ± 1	19 ± 2	11.1 ± 0.7	1.3 ± 0.6
T49	M2	0.96	...	120 ± 3	...	117 ± 2	...
CHX 18N . . .	K6	0.83	...	358 ± 4	...	196 ± 3	...
CHNR 49NE	M0	0.67	...	49 ± 2	...	18.8 ± 0.9	...
CHXR 84 . . .	M5.5	0.66	19 ± 1	14.8 ± 0.8	12 ± 2	5.5 ± 0.6	1.2^e
ISO 282 . . .	M4.75	1.04	13.2 ± 0.8	12.2 ± 0.8	10 ± 2	9.3 ± 0.7	9 ± 2
T50	M5	0.78	52 ± 2	44 ± 2	35 ± 2	39 ± 2	50 ± 4
T51	K3.5	0.75	377 ± 4	367 ± 4	344 ± 4	487 ± 5	242 ± 9
CHXR 55 . . .	K4.5	0.66	60 ± 2	38 ± 2	24 ± 2	14.0 ± 0.8	1.8 ± 0.7
Hn 18	M3.5	0.75	27 ± 1	24 ± 1	20 ± 2	19.1 ± 0.9	24 ± 3
CHXR 59 . . .	M2.75	0.74	46 ± 2	31 ± 1	19 ± 2	11.6 ± 0.7	1.2 ± 0.6
CHXR 60 . . .	M4.25	0.71	22 ± 1	17.1 ± 0.9	11 ± 2	5.4 ± 0.5	1.2^e
T55	M4.5	0.60	20 ± 1	12.8 ± 0.9	13 ± 2	4.5 ± 0.6	1.2^e
CHXR 62 . . .	M3.75	0.82	33 ± 2	23 ± 1	15 ± 2	9.3 ± 0.7	1.4 ± 0.6

^a Luhman 2004

^b 2MASS Point Source Catalog

^c IRAC data

^d MIPS data

^e upper limit

Table 2. Chamaeleon I members with accretion signatures measurements and multiplicity status

ID	SpT	H α 10% width (km s $^{-1}$)	Reference	Multiplicity	Projected separation (AU)
CHXR 12.	M3.5	110 \pm 20	1	single	...
ISO 52....	M4	107 \pm 8	1	single	...
Cha H α 12	M6.5	107	2	single	...
Hn 5.....	M4.5	340 \pm 20	1	single	...
CHXR 20.	K6	70 \pm 30	1	single	...
CHXR 74.	M3	100 \pm 20	1	single	...
T23.....	M1.5	247	2	single	...
T24.....	M0.5	430 \pm 50	1	single	...
Cha H α 1.	M7.75	151	2	single	...
Cha H α 9.	M5.5	91	2	single	...
CHXR 76.	M4.25	88 \pm 7	1	single	...
Cha H α 7.	M7.75	114	2	single	...
Cha H α 2.	M5.25	317	2	binary	\sim 25
T34.....	M3.75	90 \pm 20	1	single	...
Cha H α 13	M5.5	122	1	single	...
T35.....	K8	450 \pm 30	1	single	...
Cha H α 6.	M5.75	282	1	single	...
CHXR 33.	M0	129 \pm 2	1	single	...
CHXR 37.	K7	140 \pm 30	1	binary	\sim 11
T40.....	K6	350 \pm 40	1	single	...
CHXR 40.	M1.25	130 \pm 20	1	binary	\sim 19
ISO 217..	M6.25	334	2	single	...
T43.....	M2	170 \pm 80	1	single	...
T45.....	K8	620 \pm 30	1	binary	\sim 115
T46.....	K8	320 \pm 60	1	single	...
ISO 252..	M6	274	2	single	...
CHXR 48.	M2.5	110 \pm 10	1	single	...
T49.....	M2	280 \pm 30	1	single	...
CHX 18N.	K6	400 \pm 40	1	single	...
T50.....	M5	250 \pm 60	1	single	...
T51.....	K3.5	240 \pm 30	1	single	...
Hn 18....	M3.5	120 \pm 40	1	single	...
CHXR 59.	M2.75	130 \pm 20	1	binary	\sim 24
CHXR 60.	M4.25	100 \pm 20	1	single	...
CHXR 62.	M3.75	140 \pm 20	1	binary	\sim 19

References. — (1) Nguyen et al., in prep.;(2) Mohanty et al. 2005; Muzerolle et al. 2005